Human Molecular Genetics, 2011, Vol. 20, No. 14 **2734–2744**
doi:10.1093/hmg/ddr172
Advance Access published on April 21, 2011

A point mutation in the ubiquitin-associated domain of *SQSMT1* is sufficient to cause a Paget's disease-like disorder in mice

Anna Daroszewska[1], Robert J. van 't Hof[1], Javier A. Rojas[1], Robert Layfield[2], Euphemie Landao-Basonga[1], Lorraine Rose[1], Ken Rose[1] and Stuart H. Ralston[1,*]

[1]Rheumatic Diseases Unit, University of Edinburgh, Edinburgh EH4 2XU, UK, [2]School of Biomedical Sciences, University of Nottingham Medical School, Nottingham NG7 2UH, UK

Received December 19, 2010; Revised March 30, 2011; Accepted April 15, 2011

Mutations of *SQSTM1* occur in about 10% of patients with Paget's disease of bone (PDB), but it is unclear whether they play a causal role or regulate susceptibility to an environmental trigger. Here we show that mice with a proline to leucine mutation at codon 394 of mouse *sqstm1* (P394L), equivalent to the P392L *SQSTM1* mutation in humans, develop a bone disorder with remarkable similarity to PDB. The P394L mutant mice developed focal bone lesions with increasing age and by 12 months, 14/18 (77%) heterozygotes and 20/21 (95%) homozygotes had lesions, compared with 0/18 (0%) wild-type littermates ($P < 0.001$). Lesions predominantly affected the lower limbs in an asymmetric manner and were characterized by focal increases in bone turnover, with increased bone resorption and formation, disruption of the normal bone architecture and accumulation of woven bone. Osteoclasts within lesions were larger and more nucleated than normal and some contained nuclear inclusions similar to those observed in human PDB. Osteoclast precursors from P394L mutant mice had increased sensitivity to RANKL *in vitro* resulting in the generation of osteoclasts that were larger and more nucleated than those generated from wild-type littermates. There was increased expression of *sqstm1,* autophagy-related gene 5 (*atg5*) and light chain 3 gene (*lc3*) in osteoclast precursors and increased LC3-II protein levels in Bafilomycin-treated osteoclasts from P394L mutant mice compared with wild-type suggesting dysregulation of autophagy and enhanced autophagosome formation. These studies demonstrate that *SQSTM1* mutations can cause a PDB-like skeletal disorder in the absence of an additional trigger and provide a new disease model for PDB.

INTRODUCTION

Paget's disease of bone (PDB) is a common condition with a strong genetic component characterized by focal increases in bone turnover, which can lead to various complications, including bone pain, deformity, pathological fractures and deafness (1). Current evidence suggests that PDB is a polygenic disorder caused in part by protein-coding mutations affecting the *SQSTM1* gene which cause a dominantly inherited form of the disease which is highly penetrant (2,3) and by common variants at the *CSF1*, *TNFRSF11A* and *OPTN* loci which predispose to PDB in patients who do not carry *SQSTM1* mutations (4). Mutations affecting the *Sequestosome 1* gene (*SQSTM1*) occur in between 20 and 50% of patients with a family history of PDB, and 5 and 20% of patients with 'sporadic' disease (1). The *SQSTM1* gene encodes p62, a scaffold protein that is involved in the regulation of nuclear factor kappa B (NFκB) signalling, osteoclast formation, autophagy and apoptosis (5). Virtually, all of the PDB-associated mutations described so far lie within or are close to the ubiquitin-associated (UBA) domain of the gene product (2,3,6–9). Most of these mutations impair or abolish the ability of p62 to bind polyubiquitin chains, suggesting that this may be a unifying mechanism by which PDB occurs (10). Previous studies have shown that *SQSTM1* mutations activate NFκB signalling and enhance osteoclastogenesis *in vitro* (11–13), but the molecular mechanisms by which this occurs are incompletely understood.

*To whom correspondence should be addressed at: Rheumatic Diseases Unit, School of Molecular and Clinical Medicine, University of Edinburgh, Edinburgh EH4 2XU, UK. Tel: +44 1316511035; Fax: +44 1316511085; Email: stuart.ralston@ed.ac.uk

The penetrance of PDB in *SQSTM1* mutation carriers increases with age to reach ~80% by the seventh decade (6,14,15). Recent reports have suggested that the onset of the disease is delayed in offspring of carriers (15) and this, coupled with a decreasing incidence of the disease in some countries over the past 25 years (16,17), has led to the suggestion that *SQSTM1* mutations may not be sufficient to cause PDB and that an additional environmental trigger is required (18). Experimental evidence has been presented to suggest that infection of osteoclast precursors early in life by measles or distemper virus might act as such a trigger (18), but evidence for this is conflicting (1). The aim of this study was to determine whether *SQSTM1* mutations play a causal role in PDB by generating a mouse in which the proline residue at codon 394 of *sqstm1* is replaced by leucine (P394L), which mimics the P392L mutation of *SQSTM1*, most commonly associated with PDB in humans (14).

RESULTS

P394L mutant mice develop Pagetic-like skeletal lesions on microCT analysis

Mice carrying the P394L mutation were viable and fertile, and offspring of heterozygote mating displayed the expected Mendelian distribution of genotypes. We screened for the presence of bone lesions by performing microCT analysis focusing on the hind limbs and lumbar vertebrae. No lesions were observed in 4-month-old mice, but by 8 months, 1/4 (25%) heterozygous mice ($P394L^{+/-}$) and 7/10 (70%) homozygous mice ($P394L^{+/+}$) had developed focal osteolytic lesions mainly affecting the hind limbs compared with 0/8 (0%) wild-type littermates ($P < 0.001$). By 12 months of age, 14/18 (77%) $P394L^{+/-}$ and 20/21 (95%) $P394L^{+/+}$ mice had developed lesions compared with 0/18 wild-type littermates ($P < 0.001$). The distribution and severity of lesions are summarized in Table 1 which illustrates that the number of lesions per mouse was greater in $P394L^{+/+}$ mice when compared with $P394L^{+/-}$ mice. There was no difference in the proportion of male and female mice with lesions or in the severity of lesions between genders (data not shown). Examples of lesions visualized by 3D microCT reconstruction are shown in Figure 1B–F. The most common sites affected were the distal femur and proximal tibia close to the growth plate (Fig. 1B and C). Larger lesions were found less commonly affecting the shaft of the long bones (Fig. 1D and E). Cross-sectional analysis of the reconstructed lesions revealed disorganized bone structure within the trabecular compartment and osteolytic lesions within the cortex (Fig. 1F and G). Most lesions comprised both osteolytic and osteosclerotic components. Affected bones also showed evidence of cortical thickening and bone expansion (Fig. 1I and L), but we did not observe bending deformity of the bones as sometimes occurs in advanced human PDB. The spine was affected much less often than the tibia and femur. We identified lumbar spine lesions in one out of eight $P394L^{+/+}$ mutant mice (Fig. 1O), but no lesions were observed in eight $P394L^{+/-}$ mutant mice that we studied. In order to determine whether lesions might have developed as the result of somatic mutations, we conducted DNA sequencing of exon 8 of *sqstm1* in bone lesions from three $P394L^{+/-}$ mice and compared these results with unaffected tissue. No additional mutations of *sqstm1* within the bone lesions were detected (data not shown).

Table 1. Distribution of bone lesions in wild-type and P394L mutant mice

Site	WT ($n = 18$)	$P394L^{+/-}$ ($n = 18$)	$P394L^{+/+}$ ($n = 21$)	*P*-value
Femoral trochanter	0 (0%)	1 (5.5%)	8 (38%)	0.002
Femoral shaft	0 (0%)	2 (11%)	10 (47%)	0.001
Tibial shaft	0 (0%)	1 (5.5%)	6 (28.5%)	0.015
Distal femur or proximal tibia	0 (0%)	14 (77%)	19 (90.4%)	<0.001
Multiple sites affected	0 (0%)	7 (38.8%)	13 (61.9%)	0.001
Lesion severity score	0 (0)	1.17 ± 0.21	2.81 ± 0.36	0.001

Values are numbers and percent of animals with bone lesions at the site indicated in 12-month-old mice. Values for lesion severity score are mean ± SEM. The *P*-values refer to differences between the genotype groups as assessed by analysis of variance (ANOVA), apart from the lesion severity score which was analysed using the Kruskal–Wallis test.

Young P394L mice have normal trabecular bone density and structure

In order to establish whether the P394L mutation causes generalized abnormalities of bone mass and structure, we used microCT to examine the tibiae of 4-month-old animals, since at this point none of the mutant mice had developed focal lesions. Analysis of trabecular bone density and structure at the proximal tibial metaphysis of 4-month-old male mice revealed no significant differences in bone volume to total volume, trabecular thickness (Tb. Th), trabecular spacing (Tb. Sp) and trabecular number (Tb. N) between mutant mice and wild-type littermates (Supplementary Material, Table S1).

P394L mice exhibit focal abnormalities of bone turnover and osteoclast morphology

Histological analysis of bone lesions identified by microCT showed evidence of increased and disorganized bone turnover with disruption of normal trabecular and cortical architecture (Fig. 2A), increased numbers of osteoclasts (Fig. 2E and F) increased bone formation as detected by calcein double labelling (Fig. 2B) and woven bone as detected by polarized light microscopy (Fig. 2C and D). Bone histomorphometric analysis showed a significant increase in mineral apposition rate and mineralizing surface and a 10-fold increase in bone formation rate within the focal lesions when compared with unaffected bones (Table 2). Resorption surface and osteoclast numbers within the bone lesions were also significantly increased when compared with unaffected bone (Table 2). Examination of three focal bone lesions by transmission electron microscopy revealed the presence of nuclear inclusions in 3 of 20 osteoclasts examined, similar to those that have been observed in human PDB (19,20) (Fig. 2I and J). The inclusions consisted of multiple microcylindrical structures, or filaments arranged in a paracrystalline array which individually were ~12 nm in diameter. The dimensions are similar to that

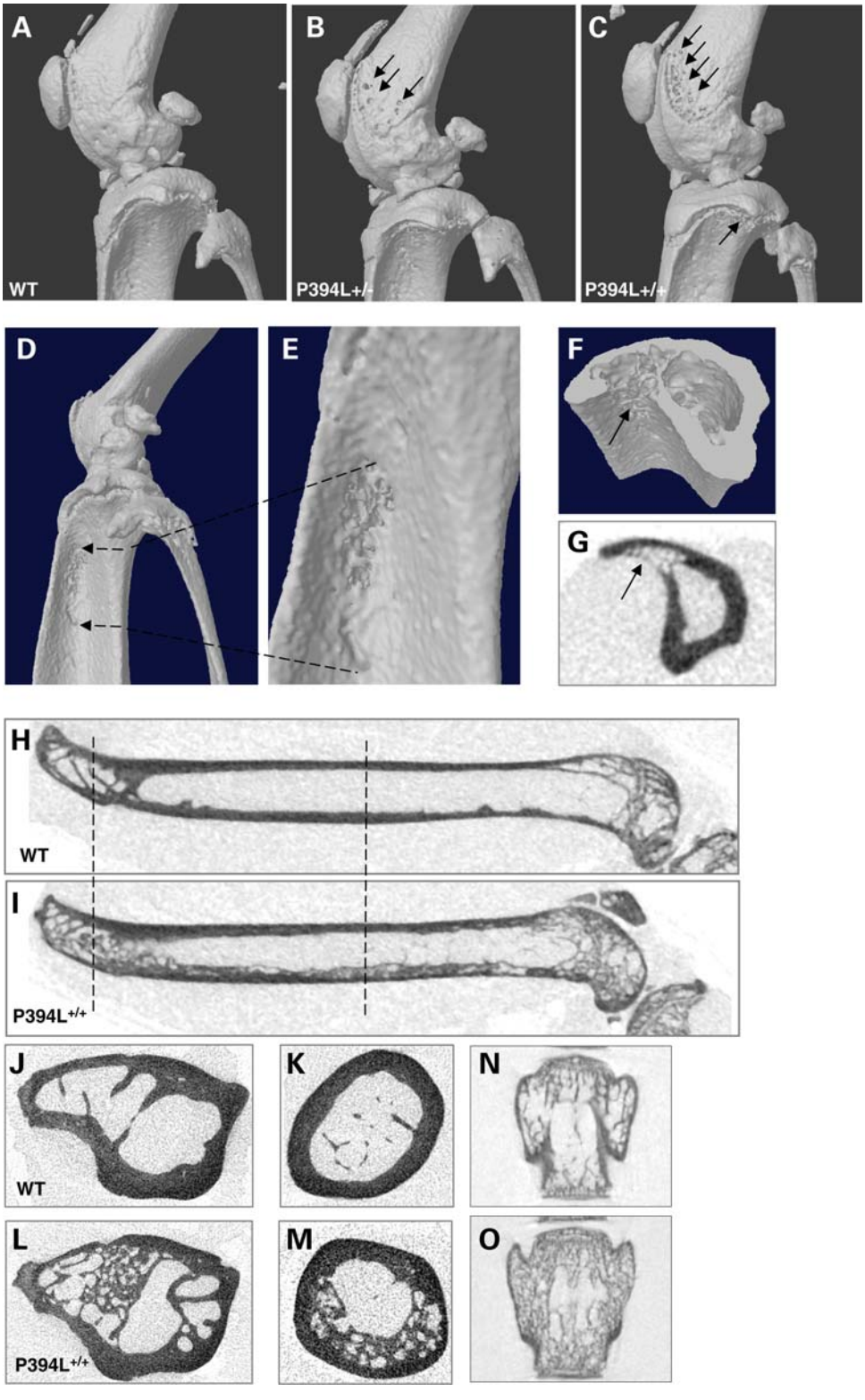

Figure 1. MicroCT analysis of long bones from P394L mutant and wild-type (WT) mice. (**A**) MicroCT analysis with 3D reconstruction of the distal femur and proximal tibia of a WT mouse, (**B**) the same area in a heterozygote P394L$^{+/-}$ mouse showing focal osteolytic lesions penetrating the cortex, (**C**) the same area in a homozygote P394L$^{+/+}$ mouse showing multiple focal osteolytic lesions penetrating the cortex, (**D**) reconstruction of a lytic lesion in the proximal aspect of the tibial shaft (arrows). (**E**) The lesion from (D) shown in greater magnification. (**F**) and (**G**) Cross-section of the lesion from (D) and (E). (**H**) Longitudinal microCT section of the femur from a WT mouse, (**I**) longitudinal microCT section of the femur from a P394L$^{+/+}$ mouse showing cortical thickening and expansion in the shaft and mixed osteosclerotic and osteolytic lesions at proximal and distal femur. (**J**–**M**) Cross-sections from the femorae of the same animals taken at the level of the broken line seen in (H) and (I). (**N**) Axial microCT image of lumbar vertebra 5 of a WT mouse showing normal morphology and trabecular structure, (**O**) lumbar vertebra 5 of a P394L$^{+/+}$ mouse showing an osteosclerotic lesion replacing most of the vertebral body.

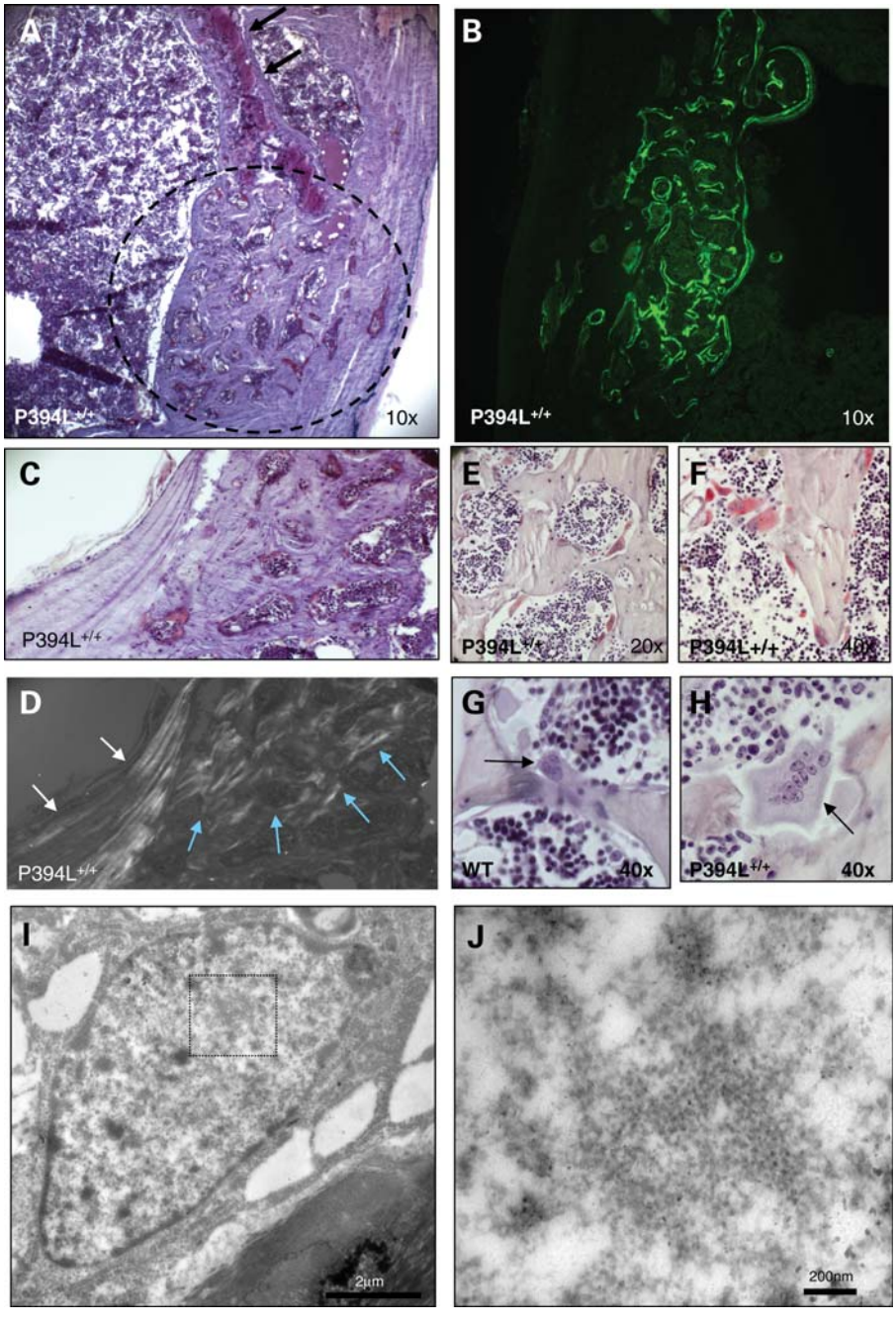

Figure 2. Histological analysis of focal lesions from P394L mutant mice. (**A**) Low power photomicrograph of bone lesion (circled) stained for tartrate resistant acid phosphatase (TRAcP) and counterstained with haematoxylin showing a mixed osteolytic and osteosclerotic lesion in the trabecular compartment and cortex. (**B**) Photomicrograph of the same lesion visualized under fluorescent light, demonstrating markedly increased rates of bone formation as reflected by the extensive calcein double labelling of bone surfaces (green) (**C**) TRAcP-stained section with a haematoxylin counterstain of a PDB-like lesion. Areas undergoing active resorption are stained red. (**D**) Same lesion seen under polarized light; the white arrows point to lamellar bone, whereas the blue arrows point to a large area of woven bone. (**E**) Photomicrograph of a lesion at ×20 magnification demonstrating increased bone resorption with multiple osteoclasts visible. (**F**) Higher power view (×40) of a different area in the same lesion. (**G**) A normal osteoclast containing three visible nuclei from a WT animal. (**H**) A large osteoclast within a lesion, containing 10 visible nuclei, from a $P394^{+/+}$ mouse. (**I**) Transmission electron micrograph (TEM) image of osteoclast nucleus from a focal bone lesion in a $P394^{+/+}$ showing nuclear inclusions consisting of multiple microcylindrical structures (dotted rectangle). (**J**) High power TEM image of the nuclear inclusion shown in (I). The diameter of individual filaments within the inclusions was ∼12 nm.

reported in human PDB where the structures have been reported to measure 12–15 nm in diameter (21). The individual osteoclasts within lesions contained significantly more nuclei than osteoclasts from unaffected bone (Figs 2H and 3). For example, 10–20% of osteoclasts from lesions in $P394L^{+/+}$ and $P394L^{+/-}$ mice contained 6–9 nuclei compared with 5% of wild-type osteoclasts and 7% of osteoclasts from unaffected bone in $P394L^{+/+}$ mice (Fig. 3). Conversely,

Table 2. Histomorphometric analysis of focal bone lesions

	WT	P394L$^{+/-}$ lesion	P394L$^{+/+}$ lesion	P394L$^{+/+}$ unaffected bone
Oc.S (%)	10.22 ± 8.91	28.82 ± 8.23***	45.73 ± 6.55***	14.07 ± 6.15###
N.Oc/BS (mm^{-1})	3.44 ± 1.74	13.15 ± 5.45***	7.30 ± 2.01***	2.81 ± 1.98##
N.Oc/TV (mm^{-2})	9.22 ± 5.83	67.43 ± 42.64***	55.91 ± 21.46**	14.21 ± 15.51##
MAR (μm/day)	2.65 ± 0.45	4.11 ± 0.84*	4.17 ± 0.54*	2.56 ± 1.11#
MS/BS (%)	18.85 ± 3.76	42.26 ± 19.96*	53.49 ± 5.35***	14.98 ± 4.34###
BFR/TV (%/day)	0.10 ± 0.045	0.94 ± 0.87*	1.58 ± 0.36***	0.11 ± 0.040###

Values are mean ± SD. Abbreviations: Oc.S, osteoclast surface; N.Oc/BS, number of osteoclasts per mm bone perimeter bone surface; N.Oc/TV, number of osteoclasts per mm^2 tissue; MAR, mineral apposition rate; MS/BS, mineralizing surface; BFR/TV, bone formation rate. Data are derived from analysis of bone lesions in seven P394L$^{+/-}$ mice and eight P394L$^{+/+}$ mice. The data for unaffected bone came from the same P394L$^{+/+}$ mice that were used for analysis of lesions. Data for the wild type (WT) mice were obtained from the proximal tibia in 10 animals which were age-matched with the P394L mutant mice. Statistical significant difference from WT mice is indicated by $^{*}P < 0.05$; $^{**}P < 0.01$; $^{***}P < 0.001$; statistical significant difference between unaffected and affected bone from P394L$^{+/+}$ mice is indicated by $^{\#}P < 0.05$; $^{\#\#}P < 0.01$; $^{\#\#\#}P < 0.001$.

70% of wild-type osteoclasts contained 1 or 2 nuclei compared with 35–45% of osteoclasts from P394L mutants (Fig. 3).

Osteoclast formation is increased in bone marrow macrophages from P394L mutant mice

Studies *in vitro* showed that M-CSF- and RANKL-induced osteoclast formation from bone marrow macrophages was significantly greater in P394L$^{+/-}$ and P394L$^{+/+}$ mice when compared with wild-type littermates (Fig. 4A–C). Moreover, osteoclast precursors from mutant mice showed evidence of increased sensitivity to RANKL when compared with wild-type cells as evidenced by the fact that osteoclast formation was observed at a RANKL concentration as low as 10 ng/ml, compared with 50 ng/ml which was necessary to reproducibly induce osteoclast formation in wild-type cells (Fig. 4C). The osteoclasts generated were larger and contained more nuclei than wild-type osteoclasts (Fig. 4D). There was no difference in osteoclast formation rate or nuclearity between P394L$^{+/-}$ and P394L$^{+/+}$ mice. Bone resorption was significantly increased in osteoclast cultures generated from both P394L$^{+/-}$ and P394L$^{+/+}$ mice resulting in a 2–3-fold increase in the total resorption area when compared with cultures prepared from wild-type mice (Fig. 4E).

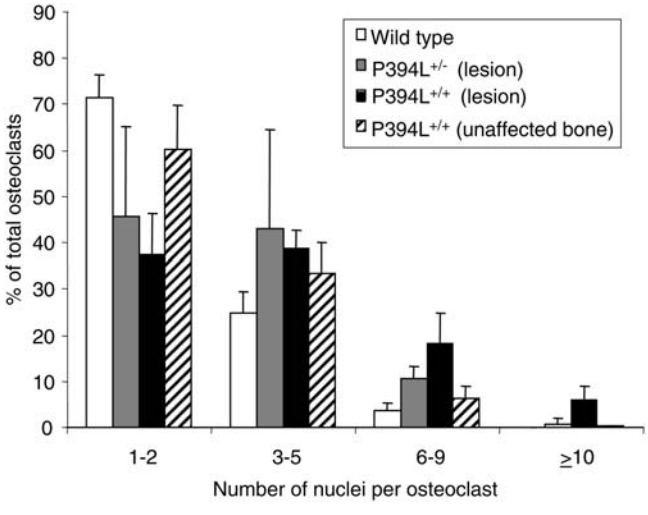

Figure 3. Osteoclasts from focal lesions in P394L mutant mice are hypernucleated. Distribution of number of nuclei per osteoclast as observed in sections stained for TRAcP and counterstained with haematoxylin. Four sections from each genotype were examined and a minimum of 50 osteoclasts per section were counted. Columns are means and bars are SD. Osteoclasts from lesions of the P394L$^{+/+}$ and P394L$^{+/-}$ mice contained significantly more nuclei than osteoclasts from the WT mice ($P < 0.0001$ and $P < 0.001$, respectively). Osteoclasts from unaffected areas from P394L$^{+/+}$ mice were not significantly different from wild-type (WT).

The P394L mutation affects autophagy in osteoclast lineage cells

We quantified levels of expression for *sqstm1*, the microtubule-associated protein 1 light chain 3 gene (*lc3*) and the autophagy-related gene 5 (*atg5*) using real-time PCR in M-CSF-dependent macrophages and osteoclast precursors derived from P394L$^{+/+}$ mice and wild-type littermates. There was a significant increase in *sqstm1*, *lc3* and *atg5* expression in the P394L$^{+/+}$ osteoclast precursors when compared with the wild-type controls; however, no significant differences in *sqstm1, lc3* and *atg5* expression were observed in P394L$^{+/+}$ and wild-type M-CSF-dependent macrophages (Fig. 5A–C).

Western blotting identified a significantly higher level of LC3-II in P394L$^{+/+}$ and P394L$^{+/-}$ osteoclasts when compared with wild-type controls after treatment with Bafilomycin A, which inhibits autophagosome–lysosome fusion (Fig. 5D and E). There was no significant difference in LC3-II levels observed in vehicle-treated P394L$^{+/+}$, P394L$^{+/-}$ and wild-type osteoclasts (Fig. 5E). Rapamycin, which induces autophagy through the inhibition of the mammalian target of rapamycin, was used as a positive control.

DISCUSSION

Here we have shown that mice that carry the P394L mutation of *sqstm1* develop a skeletal disorder with remarkable similarity to PDB. Both P394L$^{+/-}$ and P394L$^{+/+}$ mutant mice developed mixed osteolytic and osteosclerotic bone lesions predominantly targeting the distal femur and proximal tibia with increasing age, mimicking the age-related increase in penetrance of PDB that is seen in humans (14,15,22). As in human PDB, the bone lesions were asymmetrical and

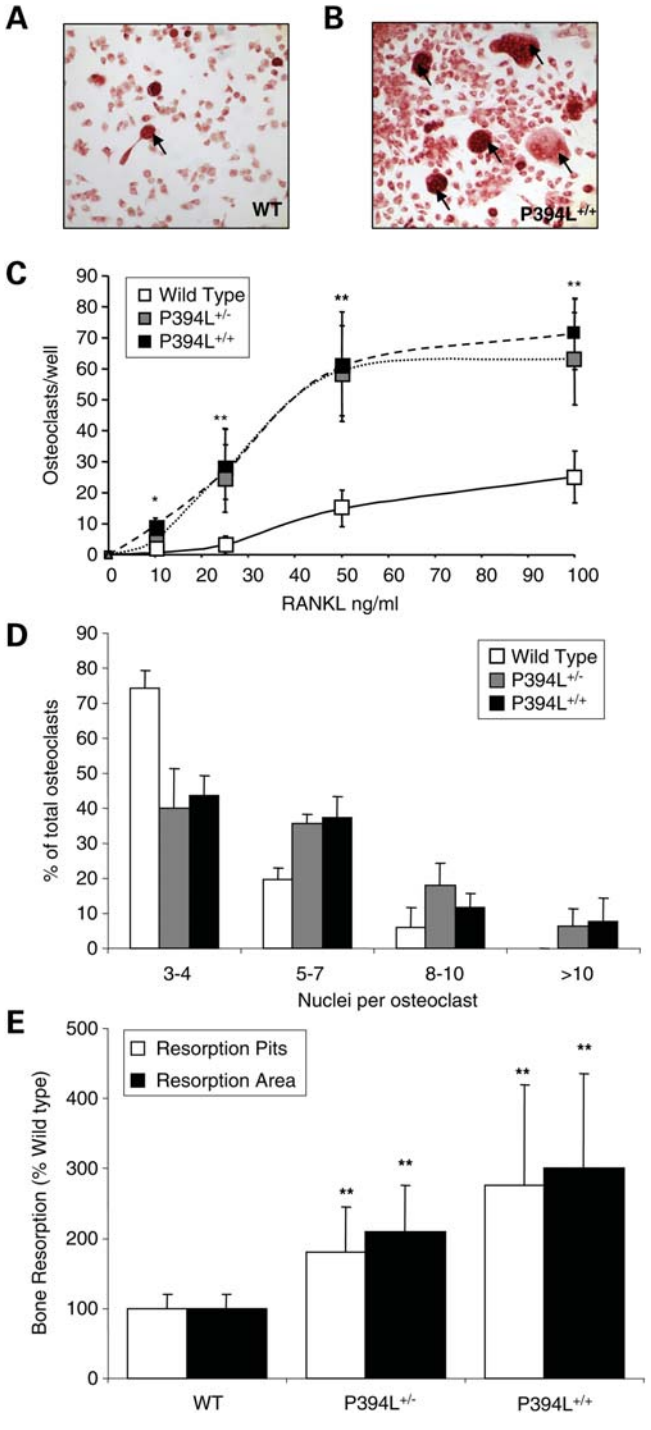

Figure 4. Osteoclast formation and nuclearity are increased in P394L mutant mice. (**A**) Photomicrographs of osteoclast cultures from M-CSF- and RANKL-stimulated macrophage cultures from wild-type (WT) mice. (**B**) Similar cultures from P394L$^{+/+}$ mutant mice. (**C**) Quantitation of osteoclast numbers in RANKL- and M-CSF-stimulated macrophage cultures from WT and P394L mutant mice. (**D**) Numbers of nuclei per osteoclast in cultures from WT and P394L mutant mice. Columns are means and bars are SD from three independent experiments. Osteoclasts from P394L$^{+/+}$ and P394L$^{+/-}$ cultures contained significantly more nuclei than osteoclasts from the WT cultures ($P < 0.01$ and $P < 0.001$, respectively). (**E**) Osteoclast cultures derived from P394L mutant bone marrow show increased resorption pit formation *in vitro*. Symbols are means and bars are SD from three independent experiments ($n = 5$ in each experiment). $^{*}P < 0.05$, $^{**}P < 0.01$ from WT cultures.

unaffected bone appeared normal as evidenced by the fact that at 4 months of age, before lesions had started to develop, microCT analysis showed no abnormalities in either P394L$^{+/-}$ or P394L$^{+/+}$ mutant mice. In keeping with this, bone histomorphometry was also normal in unaffected bone from P394L mutant mice, whereas histological analysis of bone lesions showed marked increases in bone resorption and bone formation with accumulation of woven bone. Osteoclasts were more numerous, larger and more multinucleated than normal, exactly as occurs in human PDB and some contained nuclear inclusions consisting of microcylindrical structures ~12 nm in diameter that are very similar to those that have been observed in human PDB (19–21).

The nuclear inclusions that have been observed in PDB were originally thought to represent paramyxovirus nucleocapsids (19), but their true identity is unknown and we have previously reported that Pagetic inclusions differ morphologically from those found in subacute sclerosing panencephalitis (23); the archetypical slow virus disease caused by measles virus infection (24). On the other hand, intracellular inclusions have long been recognized to be a feature of human neurodegenerative disorders such as Alzheimer's disease and Parkinson's disease which are thought to be caused in part by defects in degradation of abnormal protein aggregates by the proteasome and autophagy (5,25). Indeed, over recent years, dysregulation of autophagy has been implicated in the pathogenesis of a wide range of diseases, including neurodegenerative disorders (26,27), cancer (5) and inflammatory bowel disease (28). Autophagy is the process by which cytoplasmic protein aggregates and organelles are delivered to lysosomes for degradation (29). The autophagy-related gene 5 (ATG5), the microtubule-associated light chain 3 (LC3) and p62 are all known to play important roles in autophagy (5,30). The p62 protein plays a central role in autophagy by using its UBA domain to target polyubiquitinated proteins to the autophagic machinery by binding LC3 which is localized to the autophagosomal membrane. This results in delivery of p62 itself to autophagosomes for lysosomal degradation (29). The fact that we observed increased levels of mRNA for the *sqstm1*, *atg5* and *lc3* genes in osteoclast precursors from P394L$^{+/+}$ mice suggests that the P394L$^{+/+}$ mutation results in dysregulation of autophagy during osteoclast differentiation. Moreover, the significant elevation in LC3-II protein levels that we observed in P394L$^{+/+}$ and P394L$^{+/-}$ osteoclasts after Bafilomycin A treatment (which inhibits autophagosome–lysosome fusion) suggests that autophagosome formation may be increased as the result of this mutation, since LC3-II levels correlate with autophagosome number within the cell (30). It is therefore tempting to speculate that the nuclear inclusions observed in human PDB and in the model described here may represent abnormal protein aggregates related to abnormalities of the autophagy system, but further studies will be required to investigate this hypothesis.

Although the skeletal phenotype in mice with the P394L mutation closely resembles PDB in many respects, we acknowledge that differences also exist. For example, the proportion of P394L$^{+/-}$ mice that developed more than one lesion was ~40%, whereas we recently found that ~65% of patients with human PDB attending secondary referral centres in the UK have lesions at more that one site (31).

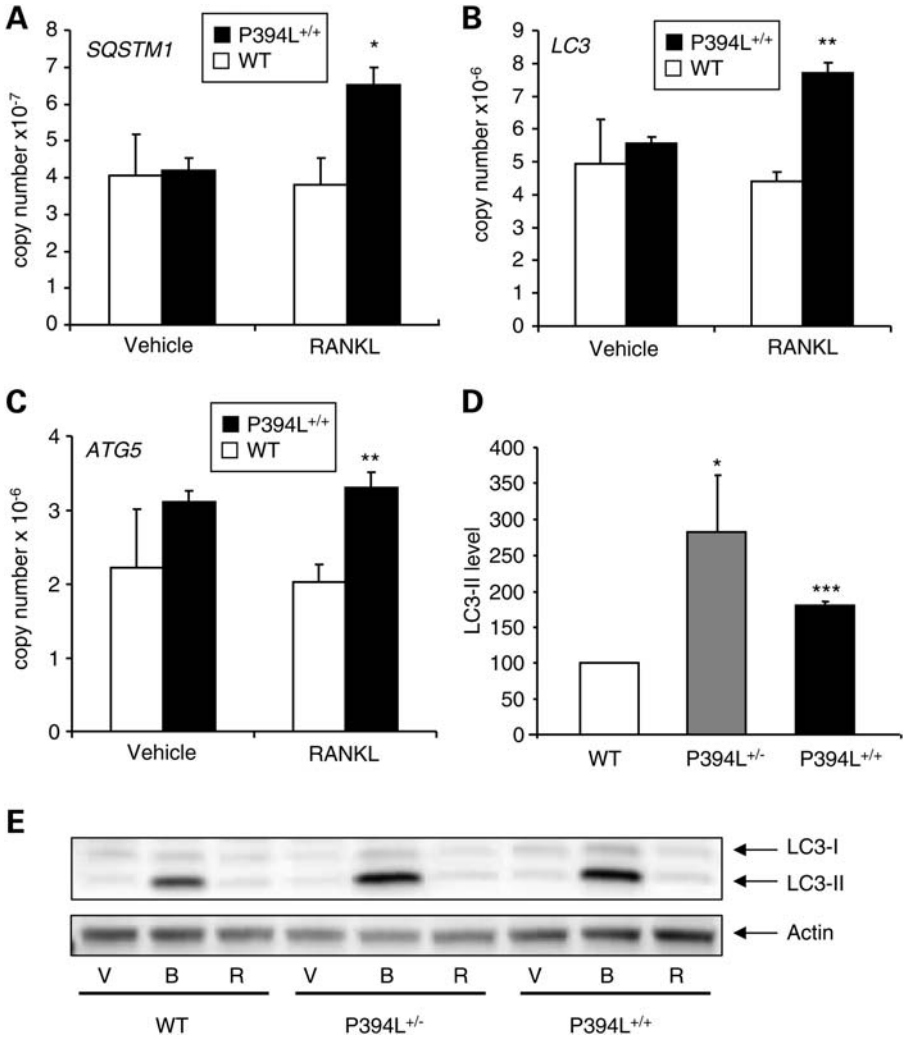

Figure 5. Increased expression of autophagy-related genes in osteoclast precursors from P394L mutant mice. (**A**–**C**) mRNA expression for the autophagy-related genes *sqstm1*, *atg5* and *lc3* in M-CSF-dependent bone marrow macrophages treated with RANKL or vehicle for 48 h. Levels of mRNA were determined by quantitative RT–PCR and are expressed as copy number per 2 μg of total RNA. The columns are means and the bars standard deviation accumulated from three independent experiments, $^{*}P < 0.05$; $^{**}P < 0.01$, P394L versus wild-type. (**D**) Levels of LC3-II corrected for actin as determined by western blotting in osteoclasts from WT, P394L$^{+/-}$ and P394L$^{+/+}$ mice treated with Bafilomycin. The data are expressed in relation to the LC3-II/actin levels in wild-type cells where the value is set at 100. The columns are means and bars are SD accumulated from three independent experiments. (**E**) shows a representative western blot from one of the experiments that contributed to the data in (D). V, vehicle-treated cultures; B, Bafilomycin-treated cultures; R, rapamycin-treated cultures. $P < 0.05$, $^{***}P < 0.001$ from wild-type cultures. Black, grey and white columns represent P394L$^{+/+}$, P394L$^{+/-}$ and WT, respectively.

However, since we screened for evidence of lesions by performing microCT restricted to the spine and lower limbs, we may have underestimated the true extent of the disease. The fact that we observed an allele dose effect of the P394L mutation on disease severity and extent is consistent with previous reports that homozygotes or compound heterozygotes for *SQSTM1* mutations generally have more severe and extensive disease than heterozygotes (22,32), although it should be noted that at least one patient homozygous for the P392L mutation had disease of similar severity to siblings who were heterozygous for the mutation (2). Another difference between the model reported here and human PDB is the distribution of lesions, which mostly occurred in the lower limbs as opposed to the axial skeleton which is predominantly affected in human PDB. This suggests that differences in the local micro-environment exist in mice which favour the development of lesions at these sites. Notably, the distal femur and proximal tibia are sites for tendon insertions into bone raising the possibility that biomechanical factors may play a role in lesion development, and this is in keeping with anecdotal reports which suggest that repetitive mechanical loading of specific bones may predispose to the development of lesions in human PDB (33,34). It is also of interest to note that these bones are commonly targeted in experimental models of metastatic bone disease and here, local increases in bone turnover and the anatomic arrangement of blood vessels in the metaphysis have been suggested to be responsible for lesion targeting (35). It is possible that one or both of these factors may have combined to give the pattern of lesion development that we observed in the present study, but further studies will be required to investigate this issue. Some researchers have reported that focal lesions in PDB

may occur as the result of somatic mutations in *SQSTM1* (36), but this was not confirmed in another study (37). In the present study, we found no evidence to suggest that additional somatic mutations of sqstm1 had occurred in bone lesions from heterozygous mice indicating that the factors discussed above were most likely responsible for the localization of bone lesions to specific regions of the skeleton.

While our study has shown that a point mutation in the UBA domain of *sqstm1* is sufficient to cause a PDB-like disorder in mice, this does not exclude the possibility that environmental factors might also influence disease severity and extent of PDB. For example, epidemiological studies have shown that the incidence and severity of PDB has decreased in the UK and New Zealand over the past 25 years (16,17), although interestingly, similar changes have not been observed in Italy (38). At present, the reason for this is incompletely understood but possibilities would include dilution of the gene pool in some localities by migrants from low prevalence areas or changes in environmental factors that influence disease severity and extent in some regions and not in others. The availability of P394L mutant mice will represent a valuable tool with which to investigate these possibilities in a rigorous fashion.

In this study, we observed that osteoclast formation and bone resorption were increased in RANKL and M-CSF stimulate bone marrow macrophages prepared from P394L mutant mice when compared with the wild-type which is in keeping with the results of previous studies which have shown that *SQSTM1* plays a key role in regulating osteoclastogenesis. For example, Duran *et al*. (39) showed that targeted disruption of *sqstm1* in mice-impaired osteoclastogenesis mediated by parathyroid hormone related protein, whereas over-expression of the P392L mutation in osteoclasts under the control of the tartrate-resistant acid phosphatase (TRAcP) promoter was found to cause a generalized increase in bone resorption and osteopenia (40). Other studies have shown that expression of the P392L variant of *SQSTM1* increases osteoclast formation and nuclearity and inhibits apoptosis in osteoclasts generated from umbilical cord-derived monocytes (13). It is of interest that Hiruma *et al.* (41) also generated mice with the P394L mutation using an approach very similar to that described here, but found no evidence of PDB-like bone lesions. In the Hiruma *et al*. (41) study, however, analysis was limited to five lumbar vertebra and the authors did not employ microCT to screen for the presence of bone lesions as we did. It seems likely that the differences in approach to phenotyping may explain the differences observed. Although Hiruma *et al.* (41) did not report evidence of increased nuclearity of P394L mutant osteoclasts, the osteoclast precursors from mutant mice were hypersensitive to RANKL and showed increased bone resorption, which is in agreement with the findings reported here.

In summary, the observations reported here are important in demonstrating that *SQSMT1* gene mutations play a causal role in the pathogenesis of PDB and provide, for the first time, an animal model of PDB. The P394L mutant mice will represent a valuable tool with which to dissect the molecular mechanisms by which *SQSTM1* mutations cause PDB; to investigate the role of environmental triggers for the disease and to investigate the pathophysiological basis by which lesions target to specific regions of the skeleton.

MATERIALS AND METHODS

Generation of SQSTM1 P394L mutant mice

To generate a mouse model for PDB associated with the *SQSTM1* P392L mutation, we employed gene targeting to generate a mouse in which the proline residue at codon 394 of the mouse Sequestosome protein was replaced by a leucine residue (P394L) (Supplementary Material, Fig. S1). In brief, the targeting construct was generated by polymerase chain reaction (PCR) and cloned into the pGEM-5Zf(+) vector. The P394L mutation was created by site-directed mutagenesis using the quick-change kit (Stratagene), and the same technique was used to insert a Spe1 site upstream of exon 8 to facilitate identification of the targeting event. The vector was further modified by cloning a polylinker into a *Bam*HI site downstream of exon 7, and this was used to insert a LoxP–Neo–LoxP cassette into the vector for positive selection. A diphtheria toxin cassette was cloned into the 3′ flank for negative selection. The plasmid was linearized with *Asc1*, purified by phenol/chloroform extraction and ethanol precipitation and transfected into E14 129/Ola embryonic stem cells by electroporation according to the standard techniques. Geneticin (200 μg/ml) was added to the culture medium after 48 h and resistant colonies were identified. These clones were initially screened for integration of the targeting vector by PCR across the 5′ and 3′ arms using primers out with the targeted region and primers within the LoxP-Neo-LoxP cassette. Clones which were positive for the recombination event on the PCR screen were further screened for correct integration using southern blotting using Spe1-digested genomic DNA. Integration of the C to T point mutation within exon 8 which results in generation of the P394L mutation was confirmed by DNA sequencing of positive clones. Cells from the positive clones were injected into recipient blastocysts from pregnant C57BL/6 females. Male chimeras generated from this procedure were mated with wild-type C57BL/6 females and germline transmission of the mutation was confirmed by genotyping of the offspring. Females from this cross were then mated with CMV-Cre expressing 129/sv males and the offspring tested for excision of the neomycin cassette by southern blotting. Males which were heterozygous for the mutation were crossed with C56BL/6 females to generate a founder colony of mice in which the P394L mutation was carried on a mixed 129/sv and C57BL/6 background. The colony was maintained by breeding heterozygotes, and the wild-type, heterozygous and homozygous animals used in this study are littermates.

MicroCT analysis

The skin was removed and hind limbs were fixed in 4% formalin-buffered saline and stored in 70% ethanol. MicroCT analysis was performed using a Skyscan 1172 system. For assessment of bone morphometry, the left tibia of 4-month-old animals was dissected free of most soft tissue, and scanned at a resolution of 5 μm (60 kV, 150 μA, using a 0.5 mm aluminium filter). The reconstruction was performed using the Skyscan NRecon package. Trabecular bone parameters were measured using Skyscan CTAn software in a stack of 200 slices immediately distal from the growth

plate as described (42). To screen for the presence of lesions, the entire limbs were initially scanned at a resolution of 16.9 μm, but more detailed scans of bones with lesions were performed at a resolution of 5 μm. Lesions were assessed independently by two observers who were blinded to the genotype. Lesions were scored according to their extension as mild (score = 1), moderate (score = 2) or severe (score = 3). All scores for each animal were added to give a total severity score per animal. The two assessors′ scores were averaged to give the final score.

Bone histology

Animals received intraperitoneal injections of calcein 4 days and 1 day before being killed. The skin was removed and the hind limbs fixed for 24 h in 4% formalin-buffered saline and stored in 70% ethanol. The samples were embedded in methyl methacrylate and 5 μm sections were cut using a tungsten steel knife. Sections were stained for TRAcP to visualize osteoclasts and counterstained with haematoxylin. Calcein double labelling was visualized on a Zeiss Axioimager fluorescence microscope fitted with a QImaging Retiga 4000R digital camera. Histomorphometry was performed using software developed in-house based on the Aphelion Image Analysis toolkit (ADCIS, France).

Transmission electron microscopy

Pagetic-like lesions were identified by microCT in two 15-month-old P394L$^{+/+}$ mice, dissected out, fixed in gluteraldehyde, decalcified and post-fixed with osmium tetroxide. The samples were embedded in Epon and sectioned. Sections were stained using lead citrate and uranyl acetate and examined using a Phillips transmission electron microscope. One section per lesion per mouse was examined and in total 20 osteoclasts were assessed for the presence of nuclear and cytoplasmic inclusions.

Osteoclast culture

Osteoclasts were generated by treatment of bone marrow macrophages with M-CSF and RANKL according to the standard methods as previously described (43). Prior to cell lysis for western blotting, osteoclasts were treated with 100 nM Bafilomycin A, or 100 nM rapamycin (Sigma-Aldrich) for 4 h. In order to obtain osteoclast precursors for RNA extraction, M-CSF-dependent macrophages were treated with RANKL for up to 48 h.

Resorption assay

Cells were flushed out of the long bones of the mice, and the resulting bone marrow cell suspension was purified using Ficoll-hypaque density-gradient centrifugation. The resulting bone marrow mononuclear cells were washed and plated at 10^5 cells per well in 16-well BD Biocoat Osteologic hydroxyapatite-coated tissue culture plates (SIS Ltd, Nottingham, UK). The cells were cultured in αMEM supplemented with 10% fetal calf serum, antibiotics and 100 ng/ml RANKL and 25 ng/ml M-CSF (R&D systems, UK). The culture medium was replaced with fresh medium every 2 days, and the plates fixed and stained using von Kossa after 10 days of culture. The stained wells were imaged using a Zeiss Axioimager microscope fitted with a using QImaging Retiga 4000R digital camera, and the resorption area was measured using the Fiji distribution of ImageJ.

Quantitative real-time PCR

Osteoclast precursors were generated in bone marrow cultures stimulated with RANKL and M-CSF for 48 h, and the RNA isolated using the Sigma GenElute™ Mammalian Total RNA Kit. RNA was quantified using the Nanodrop 1000 Spectrophotometer (Thermo Scientific) and complementary DNA was generated using the SuperScript III Reverse Transcriptase kit (Invitrogen). Primers and probes (Supplementary Material, Table S2) were designed using the Ensembl Genome Browser and the Roche website (Roche; Burgess Hill, UK). Real-time PCR was performed on a CFD-3240 Chromo 4™ Detector (M J Research) and quantified using the Opticon Monitor™ software version 3. Levels of gene expression were expressed as copy number per 2 μg of total RNA.

Western blotting

Proteins were separated by sodium dodecyl sulphate–polyacrylamide gel electrophoresis and electroblotted onto Hybond-P membranes. Membranes were blocked with 5% (w/v) non-fat milk in tris buffered saline with tween (TBST) (50 mM Tris, 150 mM NaCl, 0.1% [v/v] Tween-20) and probed with primary antibodies to LC3 (1:1000, MBL) and actin (1:1000, Sigma). After washing with TBST, membranes were incubated with appropriate horseradish peroxidise-conjugated secondary antibodies, washed and visualized using SuperSignal® West Dura Extended Duraton Substrate (Thermo Scientific) on the SynGene GeneGnome. Intensities of bands were quantified using SynGene Gene Tools software.

Statistical analyses

Statistical analyses were performed using Minitab version 12 or SPSS. For categorical variables, differences between genotype groups were determined by Chi-square test. For continuous variables, differences between genotype groups were determined by ANOVA or by the Kruskal–Wallis test followed by Dunn's post-test for data that were not normally distributed.

SUPPLEMENTARY MATERIAL

Supplementary Material is available at *HMG* online.

ACKNOWLEDGEMENTS

We acknowledge the contribution of the late Stuart Bear for expert technical assistance in histology. We thank Stephen Mitchel for expert technical assistance with the transmission electron microscopy. We also acknowledge Genoway (Lyon, France) for the gene targeting experiments.

Conflicts of Interest statement. None declared.

FUNDING

This work was supported by Arthritis Research UK (grant number 13724) and the Medical Research Council (grant numbers G0800933 and G0300413). A.D. is supported by an ECTS/AMGEN Bone Biology Fellowship from the European Calcified Tissues Society. R.L. is supported by Arthritis Research UK (grant number 18865) and the Paget's Association.

REFERENCES

1. Ralston, S.H., Langston, A.L. and Reid, I.R. (2008) Pathogenesis and management of Paget's disease of bone. *Lancet*, **372**, 155–163.
2. Laurin, N., Brown, J.P., Morissette, J. and Raymond, V. (2002) Recurrent mutation of the gene encoding sequestosome 1 (SQSTM1/p62) in Paget disease of bone. *Am. J. Hum. Genet.*, **70**, 1582–1588.
3. Hocking, L.J., Lucas, G.J.A., Daroszewska, A., Mangion, J., Olavesen, M., Nicholson, G.C., Ward, L., Bennett, S.T., Wuyts, W., Van Hul, W. *et al.* (2002) Domain specific mutations in Sequestosome 1 (SQSTM1) cause familial and sporadic Paget's disease. *Hum. Mol. Genet.*, **11**, 2735–2739.
4. Albagha, O.M., Visconti, M.R., Alonso, N., Langston, A.L., Cundy, T., Dargie, R., Dunlop, M.G., Fraser, W.D., Hooper, M.J., Isaia, G. *et al.* (2010) Genome-wide association study identifies variants at CSF1, OPTN and TNFRSF11A as genetic risk factors for Paget's disease of bone. *Nat. Genet.*, **42**, 520–524.
5. Moscat, J. and Diaz-Meco, M.T. (2009) p62 at the crossroads of autophagy, apoptosis, and cancer. *Cell*, **137**, 1001–1004.
6. Hocking, L.J., Lucas, G.J.A., Daroszewska, A., Cundy, T., Nicholson, G.C., Donath, J., Walsh, J.P., Finlayson, C., Cavey, J.R., Ciani, B. *et al.* (2004) Novel UBA domain mutations of SQSTM1 in Paget's disease of bone: genotype phenotype correlation, functional analysis and structural consequences. *J. Bone Miner. Res.*, **19**, 1122–1127.
7. Falchetti, A., Di Stefano, M., Marini, F., Ortolani, S., Ulivieri, M.F., Bergui, S., Masi, L., Cepollaro, C., Benucci, M., Di, M.O. *et al.* (2009) Genetic epidemiology of Paget's disease of bone in Italy: sequestosome1/p62 gene mutational test and haplotype analysis at 5q35 in a large representative series of sporadic and familial Italian cases of Paget's disease of bone. *Calcif. Tissue Int.*, **84**, 20–37.
8. Rea, S.L., Walsh, J.P., Ward, L., Magno, A.L., Ward, B.K., Shaw, B., Layfield, R., Kent, G.N., Xu, J. and Ratajczak, T. (2009) Sequestosome 1 mutations in Paget's disease of bone in Australia: prevalence, genotype/phenotype correlation and a novel non-UBA domain mutation (P364S) associated with increased NF-kappaB signaling without loss of ubiquitin-binding. *J. Bone Miner. Res.*, **24**, 1216–1223.
9. Johnson-Pais, T.L., Wisdom, J.H., Weldon, K.S., Cody, J.D., Hansen, M.F., Singer, F.R. and Leach, R.J. (2003) Three novel mutations in SQSTM1 identified in familial Paget's disease of bone. *J. Bone Miner. Res.*, **18**, 1748–1753.
10. Cavey, J.R., Ralston, S.H., Sheppard, P.W., Ciani, B., Gallagher, T.R., Long, J.E., Searle, M.S. and Layfield, R. (2006) Loss of ubiquitin binding is a unifying mechanism by which mutations of SQSTM1 cause Paget's disease of bone. *Calcif. Tissue Int.*, **78**, 271–277.
11. Yip, K.H., Feng, H., Pavlos, N.J., Zheng, M.H. and Xu, J. (2006) p62 ubiquitin binding-associated domain mediated the receptor activator of nuclear factor-kappaB ligand-induced osteoclast formation: a new insight into the pathogenesis of Paget's disease of bone. *Am. J. Pathol.*, **169**, 503–514.
12. Rea, S.L., Walsh, J.P., Ward, L., Yip, K., Ward, B.K., Kent, G.N., Steer, J.H., Xu, J. and Ratajczak, T. (2006) A novel mutation (K378X) in the sequestosome 1 gene associated with increased NF-kappaB signaling and Paget's disease of bone with a severe phenotype. *J. Bone Miner. Res.*, **21**, 1136–1145.
13. Chamoux, E., Couture, J., Bisson, M., Morissette, J., Brown, J.P. and Roux, S. (2009) The p62 P392L mutation linked to Paget's disease induces activation of human osteoclasts. *Mol. Endocrinol.*, **23**, 1668–1680.
14. Morissette, J., Laurin, N. and Brown, J.P. (2006) Sequestosome 1: mutation frequencies, haplotypes, and phenotypes in familial Paget's disease of bone. *J. Bone Miner. Res.*, **21**(Suppl. 2), 38–44.
15. Bolland, M.J., Tong, P.C., Naot, D., Callon, K.E., Wattie, D.J., Gamble, G.D. and Cundy, T. (2007) Delayed development of Paget's disease in offspring inheriting SQSTM1 mutations. *J. Bone Miner. Res.*, **22**, 411–415.
16. Cundy, H.R., Gamble, G., Wattie, D., Rutland, M. and Cundy, T. (2004) Paget's disease of bone in New Zealand: continued decline in disease severity. *Calcif. Tissue Int.*, **75**, 358–364.
17. Cooper, C., Schafheutle, K., Dennison, E., Kellingray, S., Guyer, P. and Barker, D. (1999) The epidemiology of Paget's disease in Britain: is the prevalence decreasing?. *J. Bone Miner. Res.*, **14**, 192–197.
18. Roodman, G.D. and Windle, J.J. (2005) Paget disease of bone. *J. Clin. Invest.*, **115**, 200–208.
19. Rebel, A., Malkani, K., Basle, M., Bregeon, C., Patezour, A. and Filmon, R. (1974) Ultrastructural characteristics of osteoclasts in Paget's disease. *Rev. Rhum. Mal. Osteoartic.*, **41**, 767–771.
20. Mills, B.G. and Singer, F.R. (1976) Nuclear inclusions in Paget's disease of bone. *Science*, **194**, 201–202.
21. Harvey, L., Gray, T., Beneton, M.N.C., Douglas, D.L., Kanis, J.A. and Russell, R.G.G. (1982) Ultrastructural features of the osteoclasts from Paget's disease of bone in relation to a viral aetiology. *J. Clin. Path.*, **35**, 771–779.
22. Eekhoff, E.W., Karperien, M., Houtsma, D., Zwinderman, A.H., Dragoiescu, C., Kneppers, A.L. and Papapoulos, S.E. (2004) Familial Paget's disease in The Netherlands: occurrence, identification of new mutations in the sequestosome 1 gene, and their clinical associations. *Arth. Rheum.*, **50**, 1650–1654.
23. Helfrich, M.H., Hobson, R.P., Grabowski, P.S., Zurbriggen, A., Cosby, S.L., Dickson, G.R., Fraser, W.D., Ooi, C.G., Selby, P.L., Crisp, A.J. *et al.* (2000) A negative search for a paramyxoviral etiology of Paget's disease of bone: molecular, immunological, and ultrastructural studies in UK patients. *J. Bone Miner. Res.*, **15**, 2315–2329.
24. Garg, R.K. (2002) Subacute sclerosing panencephalitis. *Postgrad. Med. J.*, **78**, 63–70.
25. Layfield, R., Cavey, J.R., Najat, D., Long, J., Sheppard, P.W., Ralston, S.H. and Searle, M.S. (2006) p62 mutations, ubiquitin recognition and Paget's disease of bone. *Biochem. Soc. Trans.*, **34**, 735–737.
26. Aguado, C., Sarkar, S., Korolchuk, V.I., Criado, O., Vernia, S., Boya, P., Sanz, P., de, C. Sr, Knecht, E. and Rubinsztein, D.C. (2010) Laforin, the most common protein mutated in Lafora disease, regulates autophagy. *Hum. Mol. Genet.*, **19**, 2867–2876.
27. Komatsu, M., Waguri, S., Chiba, T., Murata, S., Iwata, J., Tanida, I., Ueno, T., Koike, M., Uchiyama, Y., Kominami, E. *et al.* (2006) Loss of autophagy in the central nervous system causes neurodegeneration in mice. *Nature*, **441**, 880–884.
28. Prescott, N.J., Fisher, S.A., Franke, A., Hampe, J., Onnie, C.M., Soars, D., Bagnall, R., Mirza, M.M., Sanderson, J., Forbes, A. *et al.* (2007) A nonsynonymous SNP in ATG16L1 predisposes to ileal Crohn's disease and is independent of CARD15 and IBD5. *Gastroenterology*, **132**, 1665–1671.
29. Ravikumar, B., Sarkar, S., Davies, J.E., Futter, M., Garcia-Arencibia, M., Green-Thompson, Z.W., Jimenez-Sanchez, M., Korolchuk, V.I., Lichtenberg, M., Luo, S. *et al.* (2010) Regulation of mammalian autophagy in physiology and pathophysiology. *Physiol. Rev.*, **90**, 1383–1435.
30. Ravikumar, B., Futter, M., Jahreiss, L., Korolchuk, V.I., Lichtenberg, M., Luo, S., Massey, D.C., Menzies, F.M., Narayanan, U., Renna, M. *et al.* (2009) Mammalian macroautophagy at a glance. *J. Cell Sci.*, **122**, 1707–1711.
31. Langston, A.L., Campbell, M.K., Fraser, W.D., MacLennan, G.S., Selby, P.L. and Ralston, S.H. (2010) Randomised trial of intensive bisphosphonate treatment versus symptomatic management in Paget's disease of bone. *J. Bone Miner. Res.*, **25**, 20–31.
32. Collet, C., Michou, L., Audran, M., Chasseigneaux, S., Hilliquin, P., Bardin, T., Lemaire, I., Cornelis, F., Launay, J.M., Orcel, P. *et al.* (2007) Paget's disease of bone in the French population: novel SQSTM1 mutations, functional analysis, and genotype-phenotype correlations. *J. Bone Miner. Res.*, **22**, 310–317.
33. Solomon, L.R. (1979) Billiard-player's fingers: an unusual case of Paget's disease of bone. *Br. Med. J.*, **1**, 931.
34. Gasper, T.M. (1979) Paget's disease in a treadle machine operator [letter]. *Br. Med. J.*, **1**, 1217–1218.
35. Rosol, T.J., Tannehill-Gregg, S.H., LeRoy, B.E., Mandl, S. and Contag, C.H. (2003) Animal models of bone metastasis. *Cancer*, **97**, 748–757.

36. Merchant, A., Smielewska, M., Patel, N., Akunowicz, J.D., Saria, E.A., Delaney, J.D., Leach, R.J., Seton, M. and Hansen, M.F. (2009) Somatic mutations in SQSTM1 detected in affected tissues from patients with sporadic Paget's disease of bone. *J. Bone Miner. Res.*, **24**, 484–494.
37. Matthews, B.G., Naot, D., Bava, U., Callon, K.E., Pitto, R.P., McCowan, S.A., Wattie, D., Cundy, T., Cornish, J. and Reid, I.R. (2009) Absence of somatic SQSTM1 mutations in Paget's disease of bone. *J. Clin. Endocrinol. Metab.*, **94**, 691–694.
38. Merlotti, D., Gennari, L., Galli, B., Martini, G., Calabro, A., De Paola, V, Ceccarelli, E., Nardi, P., Avanzati, A. and Nuti, R. (2005) Characteristics and familial aggregation of Paget's disease of bone in Italy. *J. Bone Miner. Res.*, **20**, 1356–1364.
39. Duran, A., Serrano, M., Leitges, M., Flores, J.M., Picard, S., Brown, J.P., Moscat, J. and Diaz-Meco, M.T. (2004) The atypical PKC-interacting protein p62 is an important mediator of RANK-activated osteoclastogenesis. *Dev. Cell*, **6**, 303–309.
40. Kurihara, N., Hiruma, Y., Zhou, H., Subler, M.A., Dempster, D.W., Singer, F.R., Reddy, S.V., Gruber, H.E., Windle, J.J. and Roodman, G.D. (2007) Mutation of the sequestosome 1 (p62) gene increases osteoclastogenesis but does not induce Paget disease. *J. Clin. Invest.*, **117**, 133–142.
41. Hiruma, Y., Kurihara, N., Subler, M.A., Zhou, H., Boykin, C.S., Zhang, H., Ishizuka, S., Dempster, D.W., Roodman, G.D. and Windle, J.J. (2008) A SQSTM1/p62 mutation linked to Paget's disease increases the osteoclastogenic potential of the bone microenvironment. *Hum. Mol. Genet.*, **17**, 3708–3719.
42. Idris, A.I., Sophocleous, A., Landao-Bassonga, E., van't Hof, R.J. and Ralston, S.H. (2008) Regulation of bone mass, osteoclast function and ovariectomy-induced bone loss by the type 2 cannabinoid receptor. *Endocrinology*, **149**, 5619–5626.
43. Idris, A.I., Rojas, J., Greig, I.R., van't Hof, R.J. and Ralston, S.H. (2008) Aminobisphosphonates cause osteoblast apoptosis and inhibit bone nodule formation in vitro. *Calcif. Tissue Int.*, **82**, 191–201.